Title

Cell penetrating peptide functionalized perfluorocarbon nanoemulsions for targeted cell labeling and enhanced fluorine-19 MRI detection

Journal

Magnetic Resonance in Medicine, 83(3)

ISSN

0740-3194

Authors

Hingorani, Dina V
Chapelin, Fanny
Stares, Emma
et al.

Publication Date

2020-03-01

DOI

10.1002/mrm.27988

Peer reviewed

HHS Public Access

Author manuscript

Magn Reson Med. Author manuscript; available in PMC 2021 March 01.

Published in final edited form as:

Magn Reson Med. 2020 March ; 83(3): 974–987. doi:10.1002/mrm.27988.

Cell penetrating peptide functionalized perfluorocarbon nanoemulsions for targeted cell labeling and enhanced fluorine-19 MRI detection

Dina V. Hingorani[1,†], **Fanny Chapelin**[2,†], **Emma Stares**[1], **Stephen R. Adams**[3], **Hideho Okada**[4], **Eric T. Ahrens**[1,*]

[1]Department of Radiology, University of California San Diego, California 92093

[2]Department of Bioengineering, University of California San Diego, California 92093

[3]Department of Pharmacology, University of California San Diego, California 92093

[4]Department of Neurological Surgery, University of California San Francisco, California 94143

Abstract

Purpose: A bottleneck in developing cell therapies for cancer is assaying cell biodistribution, persistence and survival in vivo. Ex vivo cell labeling using perfluorocarbon (PFC) nanoemulsions, paired with ^{19}F MRI detection, is a non-invasive approach for cell product detection in vivo. Lymphocytes are small and weakly phagocytic limiting PFC labeling levels and MRI sensitivity. To boost labeling, we designed PFC nanoemulsion imaging probes displaying a cell-penetrating peptide, namely the transactivating transcription sequence (TAT) of the human immunodeficiency virus. We report optimized synthesis schemes for preparing TAT co-surfactant to complement the common surfactants used in PFC nanoemulsion preparations.

Methods: We performed ex vivo labeling of primary human chimeric antigen receptor (CAR) T cells with nanoemulsion. Intracellular labeling was validated using electron microscopy and confocal imaging. To detect signal enhancement in vivo, labeled CAR T cells were intra-tumorally injected into mice bearing flank glioma tumors.

Results: By incorporating TAT into the nanoemulsion, a labeling efficiency of ~10^{12} fluorine atoms per CAR T cell was achieved which is a >8-fold increase compared to nanoemulsion without TAT while retaining high cell viability (~84%). Flow cytometry phenotypic assays show that CAR T cells are unaltered after labeling with TAT nanoemulsion, and in vitro tumor cell killing assays display intact cytotoxic function. The ^{19}F MRI signal detected from TAT-labeled CAR T cells was eight times higher than cells labeled with PFC without TAT.

[*]**Corresponding author:** Eric T. Ahrens, University of California San Diego, 9500 Gilman Dr. #0695, La Jolla, CA 92093-0695, Phone: (858) 246-0279, eta@ucsd.edu.

Author contributions

DVH, FC, ES, SRA and ETA designed the experiments. DVH and ES synthesized materials. FC performed cell culture and histology experiments. DVH and FC performed imaging experiments. SRA provided synthesis expertise. HO provided guidance on CAR T cells. DVH and FC wrote the first manuscript draft. All authors helped edit the manuscript.

[†]Authors contributed equally

Conflict of interest disclosure

ETA is founder, consultant, member of the advisory board and shareholder of Celsense, Inc. The other authors have nothing to disclose.

Conclusion: The peptide-PFC nanoemulsion synthesis scheme presented can significantly enhance cell labeling and imaging sensitivity and is generalizable for other targeted imaging probes.

Keywords

Cell therapy; immunotherapy; cell-penetrating peptide; perfluorocarbon; fluorine-19 MRI; in vivo cytometry

INTRODUCTION

Noninvasive methods for tracking cell therapy grafts are an urgent unmet clinical need. With the development of adoptive immunotherapy against cancer, such as using chimeric antigen receptor (CAR) T cell therapy (1,2), there is a need to determine the initial biodistribution and survival of the therapeutic cells (3). Visualizing cell populations in vivo can also provide insights into off-site toxicities and help refine dosing regimens to enhance therapeutic efficacy (4,5).

Noninvasive imaging techniques for cell detection post-transfer often employ radioisotopes (6,7), bioluminescence reporters (8), and fluorescence probes (9,10). MRI is also being adapted to visualize cells (11). MRI has no depth penetration limitations, displays anatomy with clarity, and can be used with in conjunction with imaging agents clinically (12,13).

Fluorine-19 based MRI nanoemulsion probes are an option for non-invasively imaging of cell populations (14–20). The ^{19}F nuclei have high intrinsic sensitivity, with 89% relative sensitivity compared to ^{1}H. *De minimis* endogenous ^{19}F in the body ensures that any MRI signals collected are from the introduced tracer probe. F-dense perfluorocarbon (PFC) molecules are often used to form nanoemulsion imaging probes that can be endocytosed by cells. As PFCs are mostly chemically inert, lipophobic, and hydrophobic, and nanoemulsions do not osmotically diffuse out of viable cells thereby ensuring lasting labeling. Detailed reviews of the biomedical applications of ^{19}F cell detection and tracking are found elsewhere (21–24).

Engineered lymphocytes commonly used in immunotherapy (25) have an intrinsically small cytoplasmic volume and are weakly phagocytic, thereby restricting uptake of intracellular PFC label. The limits of cell detection in spin-density weighted ^{19}F MRI is linearly proportional to the cell labeling levels. Thus, to boost cell labeling, we designed PFC nanoemulsion imaging probes displaying a cell penetrating peptide (CPP) from the transactivator of transcription (TAT) component of the human immunodeficiency virus type-1 (26). TAT is an 86 amino acid protein, and residues 49–58 [Arg-Lys-Lys-Arg-Arg-Gln-Arg-Arg-Arg] are positively charged and carry a nuclear localization signal sequence facilitating endocytosis (27). We report the synthesis schemes and physical characterizations of three novel TAT co-surfactants for PFC nanoemulsion formulation. For PFC, we employ perfluoropolyether (PFPE, a perfluorinated polyethylene glycol) or perfluoro-15-crown-5-ether (PFCE); both molecules are used for ^{19}F MRI due to unitary major fluorine peaks and high sensitivity (28,29). The efficacy of TAT co-surfactants was tested by measuring cell uptake in Jurkat T cells and in human CAR T cells. In vitro functional cell (glioma) killing

assays were performed using TAT-PFC labeled CAR T cells. The intracellular localization of PFC oil droplets in labeled CAR T cells was investigated by fluorescence and electron microscopy. Additionally, we conducted proof-of-concept in vivo ^{19}F MRI sensitivity studies in CAR T cells labeled with TAT-PFC injected into flank gliomas.

METHODS

Synthesis of PFC nanoemulsions with CPP and poloxamer surfactants

To prepare CPP surfactant, 1 mmol of 1H,1H-perfluoro-1-heptanol (0.350 g, 1 mmol, mol wt = 350 g/mol) or 1H,1H-perfluoro-3,6,9-trioxadecan-1-ol (0.398 g, 1 mmol, mol wt = 398 g/mol, Exfluor Research, Round Rock, TX) was added to a 25 mL round bottom flask along with 232 mg 6-maleimidohexanoic acid (232 mg, 1.1 equiv, 1.1 mmol, mol wt = 211.32 g/mol, TCI America, Portland, OR). Anhydrous dichloromethane (5 mL) was added, and the flask was maintained under a constant stream of N_2 gas while stirring. Once the reactants dissolved, 572.4 mg benzotriazol-1-yl-oxytripyrrolidinophosphonium hexafluorophosphate (PyBOP, 572.4 mg, 1.1 equiv, 1.1 mmol, mol wt = 520.39 g/mol, Bachem, Torrance, CA) was added in one portion. After 2 min for the coupling reagent to dissolve, 350 μL of diisopropylethylamine (DIEA, 2 equiv, 2 mmol, Sigma Aldrich, St Louis, MO) was added to start the reaction. The flask was left under a slow N_2 stream with constant stirring at room temperature for 16 h. The reaction completion was monitored by thin layer chromatography (TLC, R_f = 0.4, 3:7 EtOAc: hexanes). Purification and solvent removal were accomplished using a Combiflash Rf Lumen (Teledyne Isco, Lincoln, NE) silica gel column (12 g, silica Redisep column) using a hexane and ethyl acetate gradient with 1:0 hexane:EtOAc for 3 min, followed by an increase in polarity to 1:1 hexane:EtOAc from 3 min to 14 min, followed by a 0:1 hexane:EtOAc wash for 1 min. An evaporative light scattering (ELS) detector was used for monitoring product peaks, at 250 nm and 280 nm wavelengths, which elute at retention times (t_R) = 9 min (**1**) and t_R = 10.5 min (**2**), respectively. The collected fractions were concentrated with a rotary evaporator and dried on high vacuum overnight. The products are a clear oil with mol wt = 591.28 g/mol (**1**) (yield = 325 mg) and mol wt = 543.28 g/mol (**2**) (yield = 380.1 mg).

Cys-TAT.9TFA (30 mg, 0.016 mmol, 1 equiv, mol wt = 2688.16 g/mol, Biomatik, Wilmington, DL) was dissolved in 464 μL of 0.05% TFA-water. A solution of **1** or **2** (0.014 mmol) in trifluoroethanol (556 μL) was then added to the solution of Cys-TAT, followed by the addition of 116 μL of 1 M 3-(*N*-morpholino)propanesulfonic acid (MOPS) buffer at pH = 7.4. Reaction completion was assessed by liquid chromatography mass spectroscopy (LC-MS, Model 1100 with LC/MSD Trap, Agilent, Santa Clara, CA) using a 95:5 gradient of water + 0.05% TFA: acetonitrile + 0.05% TFA for 5 min, then 95:5 to 10:90 in 20 min, followed by 10:90 to 0:100 in 10 min, t_R = 18.5 min (**1**) and t_R = 18.6 min (**2**)] and stopped after 30 min by addition of 100 μL of glacial acetic acid. Following filtration (0.22 μm nylon filter), the crude mixture was purified by semi-prep high pressure liquid chromatography [HPLC, gradients used: 90:10 descending to 10:90 water + 0.05% TFA, acetonitrile + 0.05% TFA in 20 min, t_R = 12.5 min, m/z = 1127.4, mol wt = 2254.28 g/mol (**1a, TATP**) and t_R = 13.7, m/z = 1103.5, mol wt = 2206.28 g/mol (**2a, TATA**)].

To prepare nanoemulsions, a 5% w/w ratio of total surfactant to PFC was used. For 4 mL of nanoemulsion product, 40 mg of polyethylene-polypropylene (F68) in 400 μL of water was added to a glass vial containing 465 μL PFCE (Exfluor). To this solution, 4 mg (1.21 μmol) of TATP (**1a)** or TATA (**2a**) (1.23 μmol) was added followed by 3.135 mL of purified water. The solution was ultrasonicated (30% power, 1 min, Omni Ruptor 250W, Kennesaw, GA) and then passed through a microfluidizer (LV1, Microfluidics, Westwood, MA) at 10,000 psi pressure four times. The TATA- and TATP-F68-PFC (**3**) nanoemulsions were sterile filtered using a 0.22 μm syringe filter (Acrodisc PF, Pall, Port Washington, NY) and bottled in autoclaved glass vials. The capped vials were stored at 4 °C until use.

Synthesis of PFC nanoemulsions with CPP-phospholipid surfactants

For CPP-phospholipid surfactant, 1,2-distearoyl-sn-glycero-3-phosphoethanolamine-N-[maleimide(polyethyleneglycol)-2000] (DSPE-PEG2000-maleimide, 1.8 equiv., 0.00217 mmol, 6.5 mg, Avanti Polar Lipids, Alabaster, AL) was suspended in HEPES buffer (0.05 M, 500 μL, pH = 7.5) by sonication. A fresh solution of Cys-TAT (1 equiv, 0.0012 mmol, 2.0 mg) in HEPES buffer (0.05 M, 300 μL, pH = 7.5) was added in one portion, and the mixture was agitated on a shaker at 37 °C for 6 hours. 2-Mercaptoethanol (0.8 μL, 10 equiv, 0.012 mmol, Sigma Aldrich) was added to react with any remaining maleimide groups, and the solution was agitated further for 30 min.

The conjugate was de-salted and purified in deionized water using a dialysis cassette (Slide-A-Lyzer #2K MWCO, cassette size = 3 mL, Thermo Fisher Scientific, Waltham, MA) at room temperature. Water was replaced at 2, 4 and 22 hours (volume 300:1 compared to cassette size). The sample was recovered from cassette and analyzed by matrix assisted laser desorption/ionization (MALDI) mass spectrometry (Biflex IV MALDI-TOFMS, Bruker, Billerica, MA) and identified as a mixture of the desired product, DSPE-PEG(2000)-Cys-TAT (mol wt= 4660 g/mol) **4** and DSPE-PEG(2000)-mercaptoethanol (mol wt= 3020 g/mol). The solution was lyophilized to a dry powder to give a near-quantitative yield of the desired product, **4**.

The phospholipid-PEG-TAT conjugate was incorporated into egg yolk phospholipid (EYP) by the two methods described below. For both methods, compound **1** (2.8 mg, 0.6 μmol) and EYP (304 mg, 0.4 mmol, Sigma Aldrich) were mixed resulting in a TAT to lipid surfactant ratio of 0.15 mol %. Thereafter, PFPE oil (1.18 g, 0.87 mmol, mol wt = 1300–1400 g/mol, Exfluor) was added to obtain a 26% w/w ratio of phospholipid to PFPE. Sterile water was added to obtain a 120–150 mg/mL concentration of PFPE. The nanoemulsions were then sterile-filtered through (0.2 μm, Pall) into glass vials, capped, and stored at 4 °C until use. Following formulation and filtration, each nanoemulsion was characterized by dynamic light scattering (DLS) particle analysis and ^{19}F NMR (see Supporting Information).

Method 1: Direct insertion of peptide conjugate—Compound **4** was added to a solution of EYP in chloroform (5 mL), vortexed on medium for 1 min, and the resulting solution evaporated with a stream of nitrogen while manually rotating the vessel. The vial was then placed under high vacuum overnight to give a dry lipid film. Sterile water was added to hydrate the lipid film for 5 min followed by vortexing on medium for 2 min and

then ultrasonication (30% power, 4 min). PFPE was added to the vial in one portion, vortexed briefly, and then ultrasonicated (30% power, 2 min). The crude emulsion (**5**) was passed four times through a microfluidizer at 20,000 psi with the reaction chamber cooled on ice.

Method 2: Post-insertion of peptide conjugate—A suspension of EYP in sterile water was formed by ultrasonication (30% power, 4 min), and PFPE oil was added to the vial in one portion, vortexed briefly, and then ultrasonicated (30% power, 2 min). The crude emulsion was passed four times through a microfluidizer as in method 1. To incorporate TAT, solutions of **1** based on mol% of total EYP surfactant were prepared in sterile water. The solution of **1** is added to the preformed nanoemulsion and agitated on a bioshaker at 37 °C for 5 h to obtain (**5**) nanoemulsion.

T cell preparation

The Jurkat T cell line was obtained commercially (#TIB-152, ATCC, Manassas, VA) for initial nanoemulsion cell labeling characterizations. Jurkat cells were grown in RPMI-1640 media (Gibco, Waltham, MA) plus 10% fetal bovine serum (FBS), 10 mM HEPES buffer (4-(2-hydroxyethyl)-1-piperazineethanesulfonic acid), 1 mM sodium pyruvate and 1.5 mg/mL sodium bicarbonate.

Primary human T cells were obtained from blood samples sourced from the San Diego Blood Bank and enriched for T cells by Ficoll (Histopaque 1077, Sigma Aldrich) gradient density centrifugation and magnetic assisted cell sorting (Dynabeads, Thermo Fisher). T-cells were then activated with human T-activator CD3/CD28 Dynabeads and allowed to expand for two days in RPMI-1640 supplemented with 10% FBS and 100 units/mL of recombinant human interleukin 2 (IL-2, Peprotech, Rocky Hill, NJ). For transduction, we employed a vector specific to epidermal growth factor receptor variant III (EGFR-vIII) as described by Johnson *et al.* (30). A detailed CAR virus production and human T cell transduction is available elsewhere (31). CAR receptor expression was confirmed by flow cytometry. We used T cell populations with >70% CAR+ expression.

Glioma cell line

A human glioblastoma multiform (U87-EGFRvIII-Luc) cell line overexpressing EGFR-vIII (32) and the luciferase reporter gene (Luc) were used. Cells were incubated (37 °C, 5% CO_2) and cultured in T-75 flasks (Thermo Fisher) in RPMI-1640 medium supplemented with 10% FBS.

In vitro T cell labeling

For initial uptake experiments, 1 million Jurkat or CAR T cells were plated in 1 mL full media in 24 well plates (n = 3 wells per condition). PFC nanoemulsion was added to each well and incubated overnight (16 h) at 37 °C and 5% CO_2. The cells were then washed three times with phosphate buffered saline (PBS) to remove free nanoemulsion. Cells were counted and viability was assessed by Trypan blue staining. Thereafter, the cells were spun down, resuspended in 150 μL lysis buffer (1% Triton X in PBS) and transferred to 5 mm NMR tubes. 50 μL 0.1% TFA was added to each NMR tube, and spectra were acquired (see

Supporting Information). Total fluorine atom count was divided by the sample cell number to yield the average number of fluorine atoms per cell (Supporting Information Figure S3A).

For *in vivo* experiments, CAR T cells were plated at a density of 10 million cells in 5 mL of media per well of a 6-well plate and incubated overnight with 15 mg/mL of nanoemulsion. Cells were washed as described above and an aliquot of 1 million cells was set aside to measure cell uptake by ^{19}F NMR.

Synthesis of cyanine-5 (Cy5) fluorescence nanoemulsions

TAT-PFC nanoemulsions were prepared with Cy5 dye attached (Supporting Information Figure S4). To 0.5 mmol of 1H,1H-Perfluoro-1-heptanol (mol wt = 350.08 g/mol) or 1H,1H-Perfluoro-3,6,9-trioxadecan-1-ol (mol wt = 398.08 g/mol), we added 0.55 mmol of 6-(Boc-amino)caproic acid (mol wt = 231.29 g/mol, Sigma Aldrich); this mixture was dissolved in a minimum amount of dry dichloromethane (DCM), and the reaction mix was stirred under N_2 gas. 0.55 mmol pyBOB (benzotriazol-1-yl-oxytripyrrolidinophosphonium hexafluorophosphate) was added, followed by 0.74 mmol of diisopropylethylamine (DIEA), and mixture was stirred under inert gas overnight at room temperature. Reaction completion was monitored by TLC. The solvent was removed with a rotary evaporator, and sample was dissolved in minimum amount of DCM. Wet crude sample was loaded on a 4 gm silica gel Redisep column for purification using the Combiflash Rf Lumen. We eluted with 100% hexane for 2 min, then 70%:30% EtOAc:hexane over 10 min. The desired product **6** or **7** was eluted between 30–40% EtOAc and t_R = 6–7.5 min, as monitored by ELS detector.

Boc protecting group in compound **6** or **7** was removed by adding 1 mL of TFA and 3 mL of DCM while stirring at room temperature for 1 h. The TFA was removed by forming an azeotrope with toluene, and the sample was dried under a rotary evaporator followed by high vacuum to extract all solvents. LC-MS used 10:90 to 90:10 Acetonitrile + 0.05% TFA:H_2O in 20 min. The purified compound eluted at t_R = 15.3 min, *m/z* = 515.3 (**6a**) and t_R = 16.6 min, *m/z* = 564.0 (**7a**) using the 215 nm detector.

A 25 mM stock solution of **6a** or **7a** was prepared by dissolving weighed oil in calculated amount of trifluoroethanol. We used 8 μL of 6 mM Cy5-N-hydroxysuccinimide (Cy5-NHS, 48 nmol, GE Healthcare, Chicago, IL) and an excess of **6a** or **7a** (approximately 20 equiv, 960 nmol or 38.5 μl of 25 mM stock prepared above) was added. The molar equivalent amount of N-methyl morpholine was added, prepared as a 50 mM solution in DMSO. The reaction was stirred at room temperature overnight. Thereafter, 2 μl of acetic acid was added, and the reaction mix was purified by HPLC (gradient 10:90 to 90:10 water + 0.05% TFA:Acetonitrile + 0.05% in 20 min and retain at 90:10 for an additional 10 min on a Phenomenex Luna 5 μm C18(2) 100 Å, 250 × 10 mm column). The desired product was eluted at t_R = 21.6 min, *m/z* = 1150.3 (**8**) and t_R = 20.3 min, *m/z* = 1102.3 min (**9**), as monitored by UV absorbance at 650 nm.

To prepare nanoemulsions, we used the procedure as described above. Prior to sonication, 0.3 μM of **8** is added to cocktail where TATP is used as the chosen anchor. Similarly, 0.3 μM of **9** is added to cocktail using TATA. Following sonication and microfluidization a faint blue nanoemulsion is obtained.

In vivo MRI

All animal protocols were approved by the University of California, San Diego, Institutional Animal Care and Use Committee (IACUC). Bilateral subcutaneous flank tumors were implanted in N = 4 female NOD/SCID 4–6 week old mice (Jackson Laboratories, Bar Harbor, ME). Tumor inoculant consisted of 5×10^6 U87-EGFRvIII-Luc tumor cells in 100 μL matrigel (Corning, Tewksbury, MA) in PBS (1:1). Five days later, mice received intra-tumoral injection of 1×10^7 labeled CAR T cells labeled with either TATP-F68-PFC or F68-PFC nanoemulsion. Two hours after intratumoral injection, mice were anesthetized with 1–2% isoflurane in O_2 and positioned an 11.7 T Bruker BioSpec preclinical scanner with a dual-tuned $^1H/^{19}F$ birdcage volume coil. Animal temperature was regulated, and respiration was monitored during scans. A reference capillary with dilute PFC nanoemulsion was positioned in the image field of view (FOV). ^1H anatomical images were acquired using the RARE (rapid acquisition with relaxation enhancement) sequence with TR/TE = 2000/13 ms, RARE factor 4, matrix 256×184, FOV 38×30 mm^2, slice thickness 1 mm, 18 slices, and 4 averages. The ^{19}F images were also acquired using a RARE sequence with parameters TR/TE = 1500/4.7 ms, RARE factor 8, matrix 64×46, FOV 38×30 mm^2, slice thickness 1 mm, 18 slices, and 400 averages. The total number of fluorine atoms per voxel in tumor regions were estimated directly from the *vivo* ^{19}F image hot-spots using the software program Voxel Tracker (Celsense, Pittsburgh, PA), which also employs image measurements of the external ^{19}F reference capillary signal and noise as inputs, and yields a statistical uncertainty of ^{19}F-count; additional details are published elsewhere (33). For display, ^{19}F images were manually thresholded to remove background noise, and $^1H/^{19}F$ renderings were performed in ImageJ by overlaying ^1H (grayscale) and ^{19}F (hot-iron scale) slices. Regions of interest (ROI) were segmented around relevant ^{19}F signals (right tumor, left tumor and noise), and ROI voxel intensities were displayed as histograms.

Statistical analyses

Measurements are presented as mean ± standard deviation. We performed unpaired T-tests with unequal variances to compare in vivo groups. Two tailed P-values < 0.05 were considered statistically significant.

RESULTS

Synthesis and characterization of TAT PFC nanoemulsions

To increase the cellular uptake of PFC nanoemulsion, we chemically modified and attached the TAT peptide to the surfactant to display the hydrophilic and positively charged cell penetrating moiety on the nanoemulsion surface. We tested two general methods (Figure 1) for peptide incorporation into PFC nanoemulsions; these were formed with either Pluronic F68 or phospholipid. For the poloxamer surfactant, we first conjugated TAT with a terminal cysteine (TAT-cys) directly to F68 functionalized with a maleimide group (F68-TAT, Supporting Information Figure S1)(34). Alternative PFC nanoemulsions formed with F68-TAT incorporated at ≥2% w/w of the F68 surfactant lacked long term stability and nanoemulsions that had <1% F68-TAT resulted in negligible cell uptake (data not shown). A successful approach involved conjugation of Cys-TAT to one of two small fluorous molecule anchors via a short hydrocarbon linker (Figure 1A) bearing a maleimide group that was

synthesized from the corresponding alcohols and PyBOP as a condensation agent. The two anchors consisted of either a perfluoroheptyl (TATA) or a short perfluoroPEG group (TATP), designated TATA-F68-PFC and TATP-F68-PFC, respectively, with variable percentages by weight (% w/w). Following emulsification of PFC and surfactants, both nanoemulsion formulations yielded an average size particle of 180 nm (Supporting Information Figures S2A,B) with a polydispersity index (PDI) of 0.0795–0.095, measured by light scattering methods (see Supporting Information), and particle size slightly increased by an average of 9% by day 45 post synthesis, but stabilized, and did not separate into fluorous and aqueous phases over three months (Supporting Information Figures S2C, D).

Cell labeling with TAT poloxamer nanoemulsion

Incorporation of the TAT anchored co-surfactants into F68 formulated PFC nanoemulsions resulted in significantly enhanced uptake in Jurkat cells following an 18 hour incubation (Figure 2). At low CPP stoichiometry in nanoemulsion (2.5% w/w TAT), uptake was 5.33 (±0.71) $\times 10^{11}$ ^{19}F/cell for TATP-F68-PFC and 4.67 (±0.59) $\times 10^{11}$ ^{19}F/cell for TATA-F68-PFC (dose 10 mg/ml in media, Figure 2A), measured using ^{19}F NMR of cell pellets. For higher nanoemulsion CPP content (10% w/w TATP), cell uptake was increased to 6.82 (±1.92) $\times 10^{11}$ F/cell compared to 2.25 (±0.15) $\times 10^{11}$ ^{19}F/cell for control F68-PFC nanoemulsion; similarly, TATA-F68-PFC nanoemulsion yielded uptake values of 5.26 (±0.86) $\times 10^{11}$ ^{19}F/cell (Figure 2A). Addition of either TATP or TATA did not impair cell viability (Figure 2B) as measured by permeability to Trypan blue. Incubation of Jurkat cells with TATP-F68-PFC or TATA-F68-PFC with increasing concentrations of nanoemulsion in culture displays a canonical sigmoidal uptake pattern ($p<0.01$) (Figure 2C). Activated CAR T cells labeled with TATP-F68-PFC at 15 mg/ml exhibit an average 8.2-fold uptake improvement compared to control F68-PFC-labeled cells (Figure 2E). TATA-harboring nanoemulsions exhibited mild toxicity to cells with a decrease in cell viability to 85.3% at 10 mg/mL and 83% at 20 mg/mL compared to 97.7% for untreated cells (Figure 2D). At the same doses, TATP containing nanoemulsions remained non-toxic to the cells with viability of 92% for 10 mg/mL dose and 91.7% for 20 mg/mL dose (Figure 2D).

Cell labeling with phospholipid TAT-PFC nanoemulsion

Alternative PFC nanoemulsions were also formed with EYP surfactant, where cys-TAT was conjugated to commercially available 1,2-Distearoyl-sn-glycero-3-phosphoethanolamine-peg2000-maleimide (35) (Figure 1B), and the product **4** was confirmed by Matrix Assisted Laser Desorption/Ionization mass spectrometry. Conjugate **4** was inserted into nanoemulsion either into the crude mix prior to emulsification (“direct insertion”) or after emulsification (“post-insertion”). Formed nanoemulsions containing the adduct up to 0.15 mol % (of EYP) averaged 160 nm in size with a PDI~0.2 immediately after emulsification; particle size did not change significantly over >10 weeks. No differences in size or zeta potential were observed for lipid-based nanoemulsions prepared with or without anchored TAT.

Cell labeling using TAT-modified pegylated phospholipid incorporated into EYP-surfactant nanoemulsions also resulted in greater uptake in Jurkat cells (Figure 3A). Uptake was comparable for nanoemulsions irrespective of the method of incorporation (i.e., direct insertion or post-insertion, Figure 3A). The ‘optimal’ incubation time was approximately 18

hours for 0.15 mol% phospholipid-TAT-PFC resulting in 1.23 (±0.85) $\times 10^{12}$ ^{19}F/cell. Shorter incubation times of 2 and 4 hours displayed lower uptake of 6.32 (±0.86) $\times 10^{11}$ ^{19}F/cell and 5.15 (±1.06) $\times 10^{11}$ ^{19}F/cell, respectively (Supporting Information Figure S3A). Following 18 hours of incubation, a modest reduction in cell viability was noticed and measured to be 79 (±5.65) % for phospholipid-TAT-PFC compared to 93.5 (±0.71) % for control nanoemulsion (Supporting Information Figure S3B). To test dose-dependent uptake, phospholipid-TAT-PFC (0.15 mol % of EYP) nanoemulsion was incubated with Jurkat cells for 18 hours at varying doses of 2.5, 5, 10 and 20 mg/mL. Uptake values followed a sigmoidal increase where cell uptake saturated at a dose of 10–15 mg/mL (Figure 3B), with minimal loss in cell viability even at high doses (Figure 3C).

Intracellular localization of TAT-PFC nanoemulsion in CAR T cells

We next investigated cellular localization of TATP- and TATA-F68-PFC nanoemulsions in primary T cells using high-resolution fluorescence and electron microscopy. We synthesized fluorescently labeled co-surfactants **8** and **9** consisting of Cy5 dye attached to the respective fluorous anchors (Supporting Information Figure S4) for incorporation into TATP-F68-PFC and TATA-F68-PFC nanoemulsions. Confocal microscopy of CAR T cells incubated with fluorescent nanoemulsions reveal intracellular and partial cell membrane localization of nanoemulsion (Figure 4B) compared to untreated control cells (Figure 4A); cells were co-stained with Hoechst nuclei stain and anti-CD3 fluorescent antibody for cell surface. As a further control, we tested whether the introduction of a surface dye on nanoemulsions enhanced cell uptake or caused overt cytotoxicity (Supporting Information Figure S5). The uptake of nanoemulsions formulated with dye co-surfactant are comparable to TATP-F68-PFC ($p>0.05$, Supporting Information Figure S5A), retains cell viability (Supporting Information Figure S5B), and compounds **8** and **9** do not appear to enhance internalization into live cells (Supporting Information Figure S6).

To substantiate the intracellular localization of TAT nanoemulsion in CAR T cells, electron microscopy was performed (see Supporting Information). The TATP-F68-PFC nanoemulsion droplets are present intracellularly and appear as clusters of small (~100–200 nm) punctate regions of hyperintensity in micrographs (Figures 4E, F), along with a few larger PFC deposits (~1 μm) (Figures 4G, H), presumably coalesced droplets, consistent with previous studies (29,36). Untreated control cells did not contain these hyperintense features in micrographs (Figures 4C, D). Similar findings were observed for CAR T cells labeled with TATA-F68-PFC nanoemulsion (Figures 4I–L). Normal cellular, mitochondrial and Golgi body morphologies are observed, consistent with minimal toxicity to labeled CAR T cells (Figures 4E, L) (37).

Phenotype and function of TAT-PFC labeled CAR T cells

Expression of CD3, CD4 and CD8 CAR T cell surface markers is not altered by uptake of TATA-F68-PFC and TATP-F68-PFC nanoemulsions via flow cytometry (Figure 5). Furthermore, CAR T cell killing function against glioma cells remains intact following labeling with TATP-F68-PFC nanoemulsion (Supporting Information Figure S7).

In vivo MRI of CAR T cells labeled with TAT-PFC nanoemulsion

To demonstrate the utility of TAT PFC nanoemulsion for in vivo MRI, we investigated ^{19}F signal detection from CAR T cells implanted into a rodent model. Mice bearing bilateral flank glioma tumors were injected intra-tumorally with CAR T cells (1×10^7 cells) labeled with either TATP-F68-PFC or F68-PFC (control) nanoemulsion. Figures 6A, B display spin-density weighted ^{19}F images (pseudo-color) of injected cells, along with T_2-weighted ^{1}H images (grayscale) showing tumors in flanks. We use computational post-processing of the raw (unthresholded) image data using Voxel Tracker software to analyze the apparent ^{19}F signal in vivo. The histogram in Fig. 6C represent the results of total signal detected in vivo. Figure 6C displays greater number of high intensity pixels for TAT-F68-PFC-labeled CAR T cells compared to F68-PFC-labeled CAR T cells and noise. With aid of the calibrated ^{19}F reference in the image FOV, quantification of the three-dimensional ^{19}F images was performed; the right and left tumors display (Figure 6D) 17.9 (±2.1) $\times10^{18}$ and 2.1 (±0.2) $\times10^{18}$ ^{19}F atoms per tumor, respectively, revealing a significant ($p<0.01$) 8.5-fold sensitivity improvement in detection of CAR T cells labeled with TAT PFC nanoemulsion. This sensitivity increase is predicted, based on uptake analysis by ^{19}F NMR of pelleted cells prior to injection, showing ~8.2-fold increase in average fluorine content per cell for TATP-F68-PFC versus control nanoemulsion. Of note, the ^{19}F/cell measured after labeling was observed to be greater for activated CAR T cells compared to the Jurkat cell line, ~8.2-fold and ~5-fold (Figure 2C, E), respectively, when both are labeled with TATP-F68-PFC nanoemulsion. The ^{19}F quantification results in vivo also confirm that approximately 100% of injected T cells are detected at two hours. Tumors were resected after imaging to verify intratumoral delivery of CAR T cells via extremely high-resolution ex vivo MRI (Figures 6E, F, S8).

DISCUSSION

Fluorine-19 MRI methods have shown promise for the detection of cell therapy products post-transfer (12,14–16,18,19,38), inflammatory infiltrates (39–43) and molecular targets (44) in vivo in preclinical models. Moreover, first-generation ^{19}F probes based on PFC nanoemulsions have been used in a pilot clinical trial (12). Overall, the utility of ^{19}F MRI could be expanded by increasing the sensitivity of ^{19}F probes via molecular design. Towards this goal, we aim to increase the cell adhesion and resulting endocytosis of PFC nanoemulsions by non-phagocytic cells, especially engineered lymphocytes. We synthesized three different surfactant-anchored cell penetrating TAT peptides using small molecules that either mimic the common surfactants used in emulsion formulations, namely phospholipids and poloxamers, or the fluorous environment of the nanoemulsion droplet. We compared the efficacy of poloxamer and phospholipid-based surfactants doped with TAT-conjugates and investigated nanoemulsion formation, droplet size, stability, cell uptake and viability ex vivo. Overall, nanoemulsions harboring TAT peptides led to a 4- to 8-fold cell loading improvement in T cells compared to the corresponding unmodified nanoemulsions. The droplet size, charge and initial cell safety was generally unaffected by the presence of TAT, presumably due to the low TAT to surfactant ratio in the nanoemulsions.

Phospholipid surfactants are often chosen to mimic the membranes of live cells and impart biocompatibility (45,46). Nonetheless, phospholipid-formulated nanoemulsions are prone to instability under storage conditions due to oxidation-mediated changes to the lipid (47), especially if metal ions are present, and lipid oxidation by-products may lead to cytotoxicity upon cell contact (48). Additionally, the formulation of phospholipid-based nanoemulsions requires a time consuming multi-step chemical process. For these reasons, we investigated the novel TAT conjugates for use with synthetic polymeric co-surfactants (*e.g.*, F68) in detail.

Direct conjugation of TAT to the Pluronic F68 (TAT-F68) as a co-surfactant resulted in nanoemulsion instability (data not shown), thus instead we conjugated TAT to short linear fluorous molecules via a short aliphatic hydrocarbon linker. The nanoemulsions prepared with TATP (**1a**) or TATA (**2a**) were stable for several months at 4 °C (Supporting Information Figure S2).

As anticipated, increasing the percentage of TAT on the surface of the nanoemulsions enhanced cell uptake. However, levels >20 % w/w of TAT to Pluronic surfactant resulted in increased cell-cell adhesion with formation of large cell clumps during labeling in vitro, thus a lower percent of TAT was used for further studies.

To validate internalization of the TAT nanoemulsions into CAR T cells, we prepared a comparable probe modified by the addition of a Cy5 fluorescent conjugate. The addition of this moiety did not alter the overall ^{19}F uptake levels in T cells. Fluorescence microscopy of labeled cells shows that nanoemulsion droplets are present at the cell membrane and in the cytosol, perhaps in endosomal compartments and in various stages of internalization and cellular processing in early to late endosomes (49). PFC label is retained in the cell as long as it is viable (50), and dead cell contents are taken up by the Kupffer cells of the liver (31,51). T cell mitosis tends to dilute the label in daughter cells which may limit long-term detectability.

It has been noted that the TAT peptide can translocate nanoparticles to the nucleus (27,52), however, in our microscopy studies we did not find nuclear localization of the TAT nanoemulsion probe. We note that TATP-F68-PFC-labeled cells can optionally be washed with a diluted trypsin solution to assist with removal of surface-adhered TAT nanoemulsion prior to use in vivo. Nonetheless, presumably given sufficient time for incubation, complete endocytosis of membrane-bound TAT nanoemulsion should occur. Definitive evidence for internalized nanoemulsions in small (~100–200 nm) to large vesicles (~1 μm) was provided by electron microscopy. We speculate that small vesicles eventually coalesce into larger ones to minimize their hydrophobic surface area in contact with the aqueous cytosol, as cells have no mechanism for metabolizing PFCs (53,54).

While the exact mechanism of TAT- and other CPP-mediated internalization into cells remains unknown (55). CPPs' ability to translocate molecules of various sizes from small molecules (56), proteins (57), nucleic acids and liposomes (58), many of which have been studied in vivo (59), makes their use for nanoemulsions attractive. In addition to the pre-clinical successes with TAT peptides (60–63), four compounds conjugated to TAT are

currently being tested in the clinic (64) for conditions such as myocardial infarction (65), pain (66), hearing loss (66), and inflammation (67), preliminary results of phase I clinical trials indicate that TAT peptides exhibit acceptable safety profiles.

This study offers a potential strategy to assist with tracking cell populations. Our in vivo model shows that CAR T cells carrying TAT functionalized nanoemulsions give increased ^{19}F MRI signal when injected into a tumor. Intratumoral immune cell delivery has successfully shown anti-tumor effects in mice (68) and has been considered as an approach for patients (69) as it may minimize toxicity from cytokine release syndrome upon treatment with high doses of T cells. Potential translation of this technology for human use will require additional safety testing (12). Also, there are inherent limitations of xenograft preclinical tumor models; immunological differences, artificial tumor implants, and similar tumor size in mouse models and humans, versus vastly different doses of cytotherapy delivered to these subjects, further limit extrapolation of our model findings to human use (24).

CONCLUSIONS

Overall, we have shown that incorporating the TAT cell penetrating peptide in PFC nanoemulsions significantly enhances cell uptake by lymphocytes and subsequently increased their detectability in vivo using ^{19}F MRI. These same agents should be useful for tagging other weakly phagocytic cells such as stem and progenitor cells. Moreover, the peptide-PFC nanoemulsion synthesis scheme presented is generalizable for a multitude of ex vivo and in vivo targeted ^{19}F MRI probes and offers new avenues for cellular-molecular imaging.

Supplementary Material

Refer to Web version on PubMed Central for supplementary material.

ACKNOWLEDGMENTS

We acknowledge Hongyan Xu for valuable technical assistance and Benjamin Leach for editing assistance.

Funding sources

This study was funded through National Institutes of Health grants R01-EB017271, R01-EB024015 and R21-NS083171 and the California Institute for Regenerative Medicine grant LA1-C12–06919. DVH was funded in part by the Howard Hughes Medical Institute.

REFERENCES

1. June CH, O'Connor RS, Kawalekar OU, Ghassemi S, Milone MC. CAR T cell immunotherapy for human cancer. Science 2018;359(6382):1361–1365. [PubMed: 29567707]
2. Townsend MH, Shrestha G, Robison RA, O'Neill KL. The expansion of targetable biomarkers for CAR T cell therapy. J Exp Clin Cancer Res 2018;37(1):163. [PubMed: 30031396]
3. Bonifant CL, Jackson HJ, Brentjens RJ, Curran KJ. Toxicity and management in CAR T-cell therapy. Mol Ther-Oncolytics 2016;3.
4. Chang ZL, Chen YY. CARs: Synthetic immunoreceptors for cancer therapy and beyond. Trends Mol Med 2017;23(5):430–450. [PubMed: 28416139]

5. Hartmann J, Schüßler-Lenz M, Bondanza A, Buchholz CJ. Clinical development of CAR T cells—challenges and opportunities in translating innovative treatment concepts. EMBO Mol Med 2017:e201607485.
6. Tarantal AF, Lee CCI, Kukis DL, Cherry SR. Radiolabeling human peripheral blood stem cells for positron emission tomography (PET) imaging in young rhesus monkeys. PloS ONE 2013;8(10):e77148. [PubMed: 24098579]
7. Wolfs E, Struys T, Notelaers T, Roberts SJ, Sohni A, Bormans G, Van Laere K, Luyten FP, Gheysens O, Lambrichts I. 18F-FDG labeling of mesenchymal stem cells and multipotent adult progenitor cells for PET imaging: effects on ultrastructure and differentiation capacity. J Nucl Med 2013;54(3):447–454. [PubMed: 23353687]
8. Wang X, Rosol M, Ge S, Peterson D, McNamara G, Pollack H, Kohn DB, Nelson MD, Crooks GM. Dynamic tracking of human hematopoietic stem cell engraftment using in vivo bioluminescence imaging. Blood 2003;102(10):3478–3482. [PubMed: 12946998]
9. Xiong T, Zhang Z, Liu B-F, Zeng S, Chen Y, Chu J, Luo Q. In vivo optical imaging of human adenoid cystic carcinoma cell metastasis. Oral Oncol 2005;41(7):709–715. [PubMed: 15935724]
10. Giepmans BNG, Adams SR, Ellisman MH, Tsien RY. The fluorescent toolbox for assessing protein location and function. Science 2006;312(5771):217–224. [PubMed: 16614209]
11. Ahrens ET, Bulte JW. Tracking immune cells in vivo using magnetic resonance imaging. Nat Rev Immunol 2013;13(10):755–763. [PubMed: 24013185]
12. Ahrens ET, Helfer BM, O'Hanlon CF, Schirda C. Clinical cell therapy imaging using a perfluorocarbon tracer and fluorine-19 MRI. Magn Reson Med 2014;72(6):1696–1701. [PubMed: 25241945]
13. Kircher MF, Gambhir SS, Grimm J. Noninvasive cell-tracking methods. Nat Rev Clin Oncol 2011;8(11):677–688. [PubMed: 21946842]
14. Bouchlaka MN, Ludwig KD, Gordon JW, Kutz MP, Bednarz BP, Fain SB, Capitini CM. (19)F-MRI for monitoring human NK cells in vivo. Oncoimmunology 2016;5(5):e1143996. [PubMed: 27467963]
15. Fink C, Gaudet JM, Fox MS, Bhatt S, Viswanathan S, Smith M, Chin J, Foster PJ, Dekaban GA. (19)F-perfluorocarbon-labeled human peripheral blood mononuclear cells can be detected in vivo using clinical MRI parameters in a therapeutic cell setting. Sci Rep 2018;8(1):590. [PubMed: 29330541]
16. Janjic JM, Ahrens ET. Fluorine-containing nanoemulsions for MRI cell tracking. Wires Nanomed Nanobi 2009;1(5):492–501.
17. Ku MC, Edes I, Bendix I, Pohlmann A, Waiczies H, Prozorovski T, Gunther M, Martin C, Pages G, Wolf SA, Kettenmann H, Uckert W, Niendorf T, Waiczies S. ERK1 as a therapeutic target for dendritic cell vaccination against high-grade gliomas. Mol Cancer Ther 2016;15(8):1975–1987. [PubMed: 27256374]
18. Somanchi SS, Kennis BA, Gopalakrishnan V, Lee DA, Bankson JA. In vivo (19)F-magnetic resonance imaging of adoptively transferred NK cells. Meth Mol Bio 2016;1441:317–332.
19. Srinivas M, Turner MS, Janjic JM, Morel PA, Laidlaw DH, Ahrens ET. In vivo cytometry of antigen-specific t cells using 19F MRI. Magn Reson Med 2009;62(3):747–753. [PubMed: 19585593]
20. Waiczies H, Lepore S, Janitzek N, Hagen U, Seifert F, Ittermann B, Purfurst B, Pezzutto A, Paul F, Niendorf T, Waiczies S. Perfluorocarbon particle size influences magnetic resonance signal and immunological properties of dendritic cells. PLoS ONE 2011;6(7).
21. Xander Staal OK, Mangala Srinivas. Chapter 11: In vivo 19-fluorine magnetic resonance imaging In: Günter Haufe FRL, editor. Fluorine in Life Sciences: Pharmaceuticals, Medicinal Diagnostics, and Agrochemicals; 2019 (Elsevier).
22. Ruiz-Cabello J, Barnett BP, Bottomley PA, Bulte JWM. Fluorine (19F) MRS and MRI in biomedicine. NMR in Biomed 2011;24(2):114–129.
23. Ahrens ET, Zhong J. In vivo MRI cell tracking using perfluorocarbon probes and fluorine-19 detection. NMR in Biomed 2013;26(7):860–871.
24. Chapelin F, Capitini CM, Ahrens ET. Fluorine-19 MRI for detection and quantification of immune cell therapy for cancer. J Immunother Cancer 2018;6(1):105. [PubMed: 30305175]

25. Lim WA, June CH. The principles of engineering immune cells to treat cancer. Cell 2017;168(4): 724–740. [PubMed: 28187291]
26. Lindgren M, Hällbrink M, Prochiantz A, Langel Ü. Cell-penetrating peptides. Trends Pharmacol Sci 2000;21(3):99–103. [PubMed: 10689363]
27. Vives E, Brodin P, Lebleu B. A truncated HIV-1 Tat protein basic domain rapidly translocates through the plasma membrane and accumulates in the cell nucleus. J Biol Chem 1997;272(25): 16010–16017. [PubMed: 9188504]
28. Janjic JM, Srinivas M, Kadayakkara DK, Ahrens ET. Self-delivering nanoemulsions for dual fluorine-19 MRI and fluorescence detection. J Am Chem Soc 2008;130(9):2832–2841. [PubMed: 18266363]
29. Ahrens ET, Flores R, Xu H, Morel PA. In vivo imaging platform for tracking immunotherapeutic cells. Nat Biotechnol 2005;23(8):983–987. [PubMed: 16041364]
30. Johnson LA, Scholler J, Ohkuri T, Kosaka A, Patel PR, McGettigan SE, Nace AK, Dentchev T, Thekkat P, Loew A. Rational development and characterization of humanized anti–EGFR variant III chimeric antigen receptor T cells for glioblastoma. Sci Transl Med 2015;7(275):275ra222.
31. Chapelin F, Gao S, Okada H, Weber TG, Messer K, Ahrens ET. Fluorine-19 nuclear magnetic resonance of chimeric antigen receptor T cell biodistribution in murine cancer model. Sci Rep 2017;7(1):17748. [PubMed: 29255242]
32. Ohno M, Ohkuri T, Kosaka A, Tanahashi K, June CH, Natsume A, Okada H. Expression of miR-17–92 enhances anti-tumor activity of T-cells transduced with the anti-EGFRvIII chimeric antigen receptor in mice bearing human GBM xenografts. J Immunother Cancer 2013;1:21. [PubMed: 24829757]
33. Srinivas M, Morel PA, Ernst LA, Laidlaw DH, Ahrens ET. Fluorine-19 MRI for visualization and quantification of cell migration in a diabetes model. Magn Reson Med 2007;58(4):725–734. [PubMed: 17899609]
34. Howard MD, Hood ED, Greineder CF, Alferiev IS, Chorny M, Muzykantov V. Targeting to endothelial cells augments the protective effect of novel dual bioactive antioxidant/anti-inflammatory nanoparticles. Mol Pharm 2014;11(7):2262–2270. [PubMed: 24877560]
35. Hu S, Wang T, Pei X, Cai H, Chen J, Zhang X, Wan Q, Wang J. Synergistic enhancement of antitumor efficacy by PEGylated Multi-walled carbon nanotubes modified with cell-penetrating peptide TAT. Nanoscale Res Lett 2016;11(1):452. [PubMed: 27726120]
36. Hitchens TK, Liu L, Foley LM, Simplaceanu V, Ahrens ET, Ho C. Combining perfluorocarbon and superparamagnetic iron-oxide cell labeling for improved and expanded applications of cellular MRI. Magn Reson Med 2015;73(1):367–375. [PubMed: 24478194]
37. van Eeden SF, Klut Me Fau - Leal MA, Leal Ma Fau - Alexander J, Alexander J Fau - Zonis Z, Zonis Z Fau - Skippen P, Skippen P. Partial liquid ventilation with perfluorocarbon in acute lung injury: light and transmission electron microscopy studies. Am J Respir Cell Mol Biol 2000;22(4): 441–450. [PubMed: 10745025]
38. Gonzales C, Yoshihara HA, Dilek N, Leignadier J, Irving M, Mieville P, Helm L, Michielin O, Schwitter J. In-vivo detection and tracking of T cells in various organs in a melanoma tumor model by 19F-fluorine MRS/MRI. PLoS One 2016;11(10):e0164557. [PubMed: 27736925]
39. Flogel U, Su S, Kreideweiss I, Ding ZP, Horning A, Witzke O, Schrader J. Early detection of transplant rejection by in vivo 19F MRI. Circulation 2009;120(18):S817–S817.
40. Ahrens ET, Young WB, Xu H, Pusateri LK. Rapid quantification of inflammation in tissue samples using perfluorocarbon emulsion and fluorine-19 nuclear magnetic resonance. Biotechniques 2011;50(4):229–234. [PubMed: 21548906]
41. Khurana A, Chapelin F, Xu H, Acevedo JR, Molinolo A, Nguyen Q, Ahrens ET. Visualization of macrophage recruitment in head and neck carcinoma model using fluorine-19 magnetic resonance imaging. Magn Reson Med 2018;79(4):1972–1980. [PubMed: 28748562]
42. Kadayakkara DK, Ranganathan S, Young WB, Ahrens ET. Assaying macrophage activity in a murine model of inflammatory bowel disease using fluorine-19 MRI. Lab Invest 2012;92(4):636–645. [PubMed: 22330343]
43. Zhong J, Narsinh K, Morel PA, Xu H, Ahrens ET. In Vivo Quantification of inflammation in experimental autoimmune encephalomyelitis rats using Fluorine-19 magnetic resonance imaging

reveals immune cell recruitment outside the nervous system. PLoS One 2015;10(10):e0140238. [PubMed: 26485716]

44. Temme S, Grapentin C, Quast C, Jacoby C, Grandoch M, Ding Z, Owenier C, Mayenfels F, Fischer JW, Schubert R, Schrader J, Flogel U. Noninvasive imaging of early venous thrombosis by 19F magnetic resonance imaging with targeted perfluorocarbon nanoemulsions. Circulation 2015;131(16):1405–1414. [PubMed: 25700177]
45. Grapentin CFriederike M; Sabine Barnert; Süss A, Schubert Regine, Temme Rolf, Jacoby Sebastian, Schrader Christoph, Juergen; Ulrich Flögel. Optimization of perfluorocarbon nanoemulsions for molecular imaging by 19 F MRI In: Nanomedicine. Edited by Seifalin A, de Mel A, Kalaskar DM; One Central Press, Manchester 2014: 268–286.
46. Temme S, Baran P, Bouvain P, Grapentin C, Kramer W, Knebel B, Al-Hasani H, Moll JM, Floss D, Schrader J, Schubert R, Flogel U, Scheller J. Synthetic cargo internalization receptor system for nanoparticle tracking of individual cell populations by fluorine magnetic resonance imaging. ACS Nano 2018;12(11):11178–11192. [PubMed: 30372619]
47. Girotti AW. Mechanisms of lipid peroxidation. J Free Radic Biol Med 1985;1(2):87–95. [PubMed: 3915303]
48. Schaich KM. Metals and lipid oxidation. Contemporary issues. Lipids 1992;27(3):209–218. [PubMed: 1522766]
49. Fretz M, Jin J, Conibere R, Penning NA, Al-Taei S, Storm G, Futaki S, Takeuchi T, Nakase I, Jones AT. Effects of Na+/H+ exchanger inhibitors on subcellular localisation of endocytic organelles and intracellular dynamics of protein transduction domains HIV–TAT peptide and octaarginine. J Control Release 2006;116(2):247–254. [PubMed: 16971016]
50. Patrick MJ, Janjic JM, Teng H, O'Hear MR, Brown CW, Stokum JA, Schmidt BF, Ahrens ET, Waggoner AS. Intracellular pH measurements using perfluorocarbon nanoemulsions. J Am Chem Soc 2013;135(49):18445–18457. [PubMed: 24266634]
51. Castro O, Nesbitt AE, Lyles D. Effect of a perfluorocarbon emulsion (Fluosol-DA) on reticuloendothelial system clearance function. Am J Hematol 1984;16(1):15–21. [PubMed: 6695906]
52. de la Fuente JM, Berry CC. Tat peptide as an efficient molecule to translocate gold nanoparticles into the cell nucleus. Bioconjug Chem 2005;16(5):1176–1180. [PubMed: 16173795]
53. Krafft MP. Fluorocarbons and fluorinated amphiphiles in drug delivery and biomedical research. Adv Drug Deliv Rev 2001;47(2–3):209–228. [PubMed: 11311993]
54. Krafft MP, Riess JG. Perfluorocarbons: Life sciences and biomedical uses dedicated to the memory of Professor Guy Ourisson, a true RENAISSANCE man. J Polym Sci Pol Chem 2007;45(7):1185–1198.
55. Brooks H, Lebleu B, Vivès E. Tat peptide-mediated cellular delivery: back to basics. Adv Drug Deliv Rev 2005;57(4):559–577. [PubMed: 15722164]
56. Mazel M, Clair P, Rousselle C, Vidal P, Scherrmann J-M, Mathieu D, Temsamani J. Doxorubicin-peptide conjugates overcome multidrug resistance. Anti-cancer Drugs 2001;12(2):107–116. [PubMed: 11261883]
57. Fawell S, Seery J, Daikh Y, Moore C, Chen LL, Pepinsky B, Barsoum J. Tat-mediated delivery of heterologous proteins into cells. Proc Natl Acad Sci 1994;91(2):664–668. [PubMed: 8290579]
58. Torchilin VP, Levchenko TS, Rammohan R, Volodina N, Papahadjopoulos-Sternberg B, D'Souza GGM. Cell transfection in vitro and in vivo with nontoxic TAT peptide-liposome–DNA complexes. Proc Natl Acad Sci 2003;100(4):1972–1977. [PubMed: 12571356]
59. Foged C, Nielsen HM. Cell-penetrating peptides for drug delivery across membrane barriers. Expert Opin Drug Deliv 2008;5(1):105–117. [PubMed: 18095931]
60. Boisguerin P, Redt-Clouet C, Franck-Miclo A, Licheheb S, Nargeot J, Barrère-Lemaire S, Lebleu B. Systemic delivery of BH4 anti-apoptotic peptide using CPPs prevents cardiac ischemia–reperfusion injuries in vivo. J Control Release 2011;156(2):146–153. [PubMed: 21839124]
61. Borsello T, Clarke PGH, Hirt L, Vercelli A, Repici M, Schorderet DF, Bogousslavsky J, Bonny C. A peptide inhibitor of c-Jun N-terminal kinase protects against excitotoxicity and cerebral ischemia. Nat Med 2003;9(9):1180. [PubMed: 12937412]

62. Michiue H, Eguchi A, Scadeng M, Dowdy SF. Induction of in vivo synthetic lethal RNAi responses to treat glioblastoma. Cancer Biol Ther 2009;8(23):2304–2311.

63. Yang D, Sun Y-Y, Lin X, Baumann JM, Dunn RS, Lindquist DM, Kuan C-Y. Intranasal delivery of cell-penetrating anti-NF-κB peptides (Tat-NBD) alleviates infection-sensitized hypoxic–ischemic brain injury. Exp Neurol 2013;247:447–455. [PubMed: 23353638]

64. Direct Inhibition of delta-Protein Kinase CEtLTISiAMII, Bates E, Bode C, Costa M, Gibson CM, Granger C, Green C, Grimes K, Harrington R, Huber K, Kleiman N, Mochly-Rosen D, Roe M, Sadowski Z, Solomon S, Widimsky P. Intracoronary KAI-9803 as an adjunct to primary percutaneous coronary intervention for acute ST-segment elevation myocardial infarction. Circulation 2008;117(7):886–896. [PubMed: 18250271]

65. Cousins MJ, Pickthorn K, Huang S, Critchley L, Bell G. The safety and efficacy of KAI-1678- an inhibitor of epsilon protein kinase C (epsilonPKC)-versus lidocaine and placebo for the treatment of postherpetic neuralgia: a crossover study design. Pain Med 2013;14(4):533–540. [PubMed: 23438341]

66. Suckfuell M, Lisowska G, Domka W, Kabacinska A, Morawski K, Bodlaj R, Klimak P, Kostrica R, Meyer T. Efficacy and safety of AM-111 in the treatment of acute sensorineural hearing loss: a double-blind, randomized, placebo-controlled phase II study. Otol Neurotol 2014;35(8):1317–1326. [PubMed: 24979398]

67. Deloche C, Lopez-Lazaro L, Mouz S, Perino J, Abadie C, Combette JM. XG-102 administered to healthy male volunteers as a single intravenous infusion: a randomized, double-blind, placebo-controlled, dose-escalating study. Pharmacol Res Perspect 2014;2(1):e00020. [PubMed: 25505576]

68. Tatsumi T, Huang J, Gooding WE, Gambotto A, Robbins PD, Vujanovic NL, Alber SM, Watkins SC, Okada H, Storkus WJ. Intratumoral delivery of dendritic cells engineered to secrete both interleukin (IL)-12 and IL-18 effectively treats local and distant disease in association with broadly reactive Tcl-type immunity. Cancer Res 2003;63(19):6378–6386. [PubMed: 14559827]

69. Ngwa W, Irabor OC, Schoenfeld JD, Hesser J, Demaria S, Formenti SC. Using immunotherapy to boost the abscopal effect. Nat Rev Cancer 2018;18(5):313–322. [PubMed: 29449659]

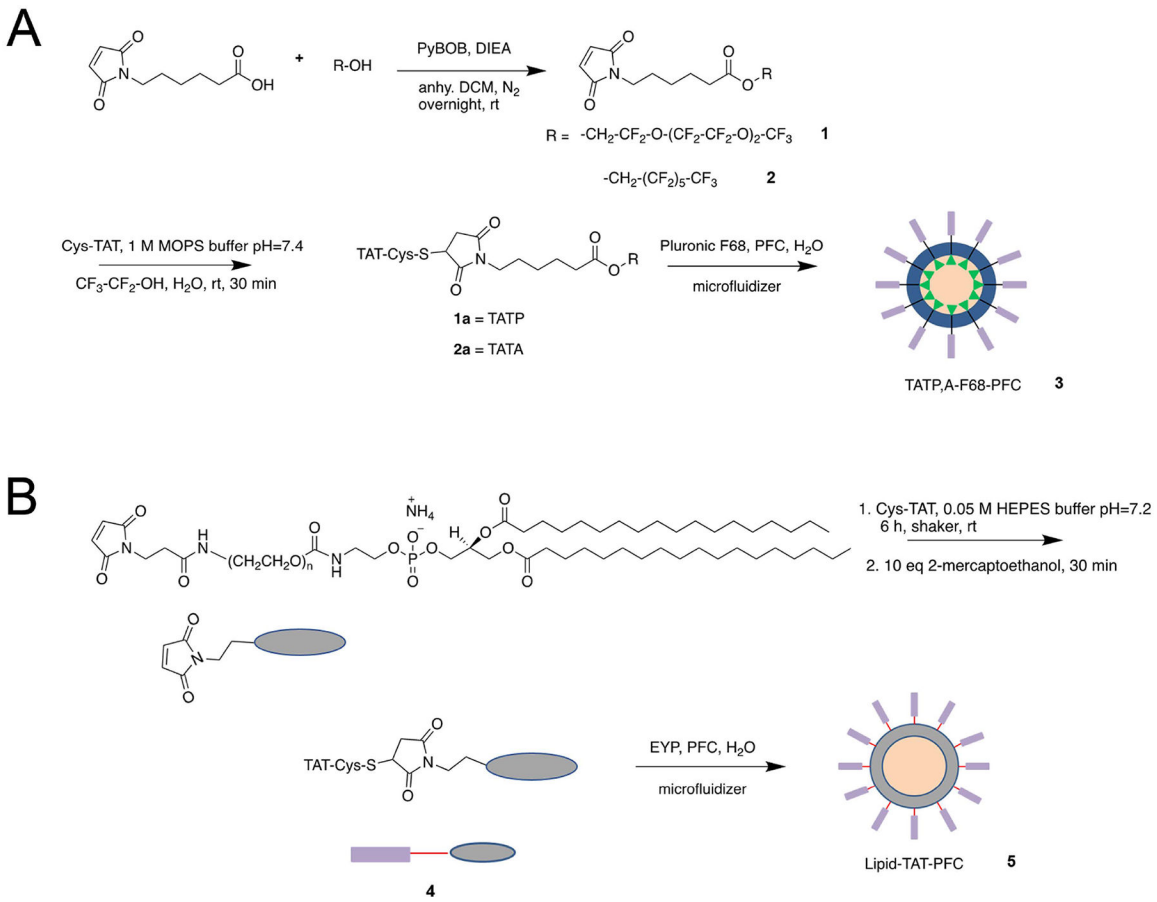

Figure 1.

Synthesis of TAT functionalized perfluorocarbon nanoemulsions. Panel (**A**) displays synthesis of TAT conjugates with fluorous anchors, TATP and TATA and poloxamer surfactant formulated nanoemulsions. Panel (**B**) shows scheme for TAT-phospholipid anchor conjugation for EYP surfactant formulated nanoemulsions.

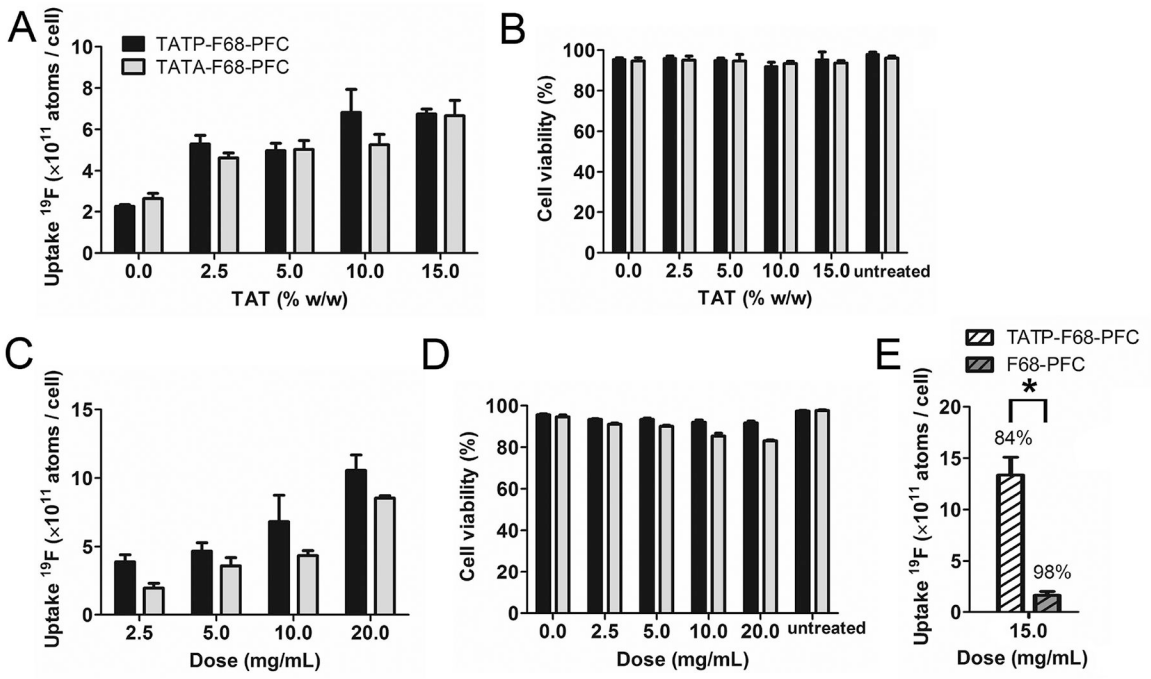

Figure 2.

T cell labeling with TATA-F68-PFC and TATP-F68-PFC nanoemulsions. The TAT anchor stoichiometry is optimized by measuring uptake (**A**) and viability (**B**) in Jurkat cells while varying the percent by weight of TAT in Pluronic surfactant PFC nanoemulsion, namely TATP-F68-PFC (black bars) and TATA-F68-PFC (grey bars). No significant differences are noted. Cell uptake (**C**) and viability **(D)** for varying dosages (in mg/mL) of 10% w/w TATP-F68-PFC and TATA-F68-PFC after 18 hour incubation are shown ($p<0.01$, uptake TATP-F68-PFC and TATA-F68-PFC. No significant differences are noted for viability). CAR T cells labeled using the same conditions exhibit an 8.2-fold uptake improvement compared to control F68-PFC labeled cells at a dose of 15 mg/ml (dashed bars, * indicates $p<0.001$, **E**). The viability of labeled CAR T cells is displayed above the bar graph. Uptake was measured from ^{19}F NMR spectra of cell pellets, and viability was measured by the Trypan blue assay and direct cell counts.

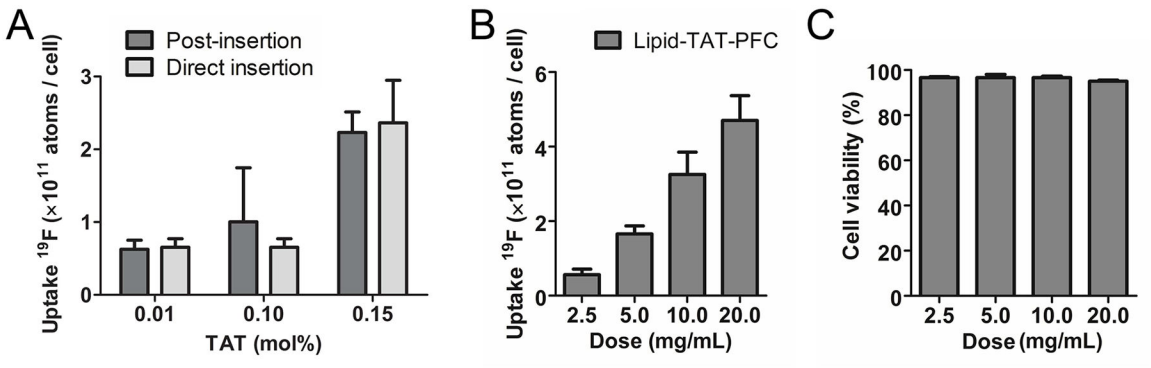

Figure 3.

Jurkat T cell labeling with lipid-TAT-PFC nanoemulsion. The TAT anchor stoichiometry is optimized by measuring uptake (**A**) in cells while varying the percent by molarity of TAT in phospholipid surfactant nanoemulsions using two different methods of preparation including post-insertion (dark grey) and direct insertion (light grey) of TAT conjugate. There is no statistical difference between the two insertion methods. The cell uptake (**B**) and viability (**C**) with varying dosage of 0.1 mol% lipid-TAT-PFC after 18 hour incubation are displayed. No significant viability impairment is noted.

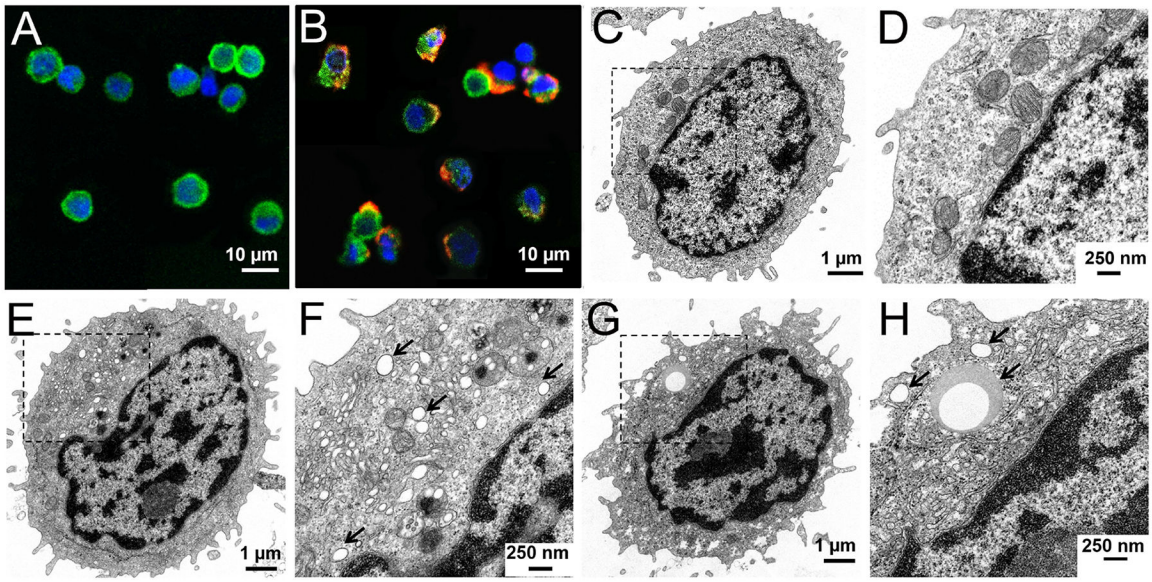

Figure 4.

Microscopy of CAR T cells labeled with TAT-F68-PFC nanoemulsions. Confocal microscopy images of untreated CAR T cells are displayed in (**A**), and CAR T cells labeled with (15 mg/mL) of Cy5-TATP-F68-PFC nanoemulsions (red) are shown in (**B**). Data show intracellular localization of Cy5-TATP-F68-PFC emulsion, where Hoechst dye (blue) stains nuclei and Alexa488 anti-human CD3 antibody (green) delineates cell membrane. Electron microscopy of untreated CAR T cells is shown in (**C**) and magnified in (**D**). CAR T cells labeled with TATP-F68-PFC (**E-H**) show numerous bright ~100 nm nanoemulsion droplets (**E,** magnified in **F**, arrows) and occasional ~1 μm coalesced droplets (**G,** magnified in **H**, arrows). CAR T cells labeled with TATA-F68-PFC (**I-L**) show similar nanoemulsion droplets as with TATP-F68-PFC nanoemulsion. Large coalesced droplets (**I,** inset **J**) as well as numerous smaller droplets (**K,** inset **L**) are found in the cytoplasm.

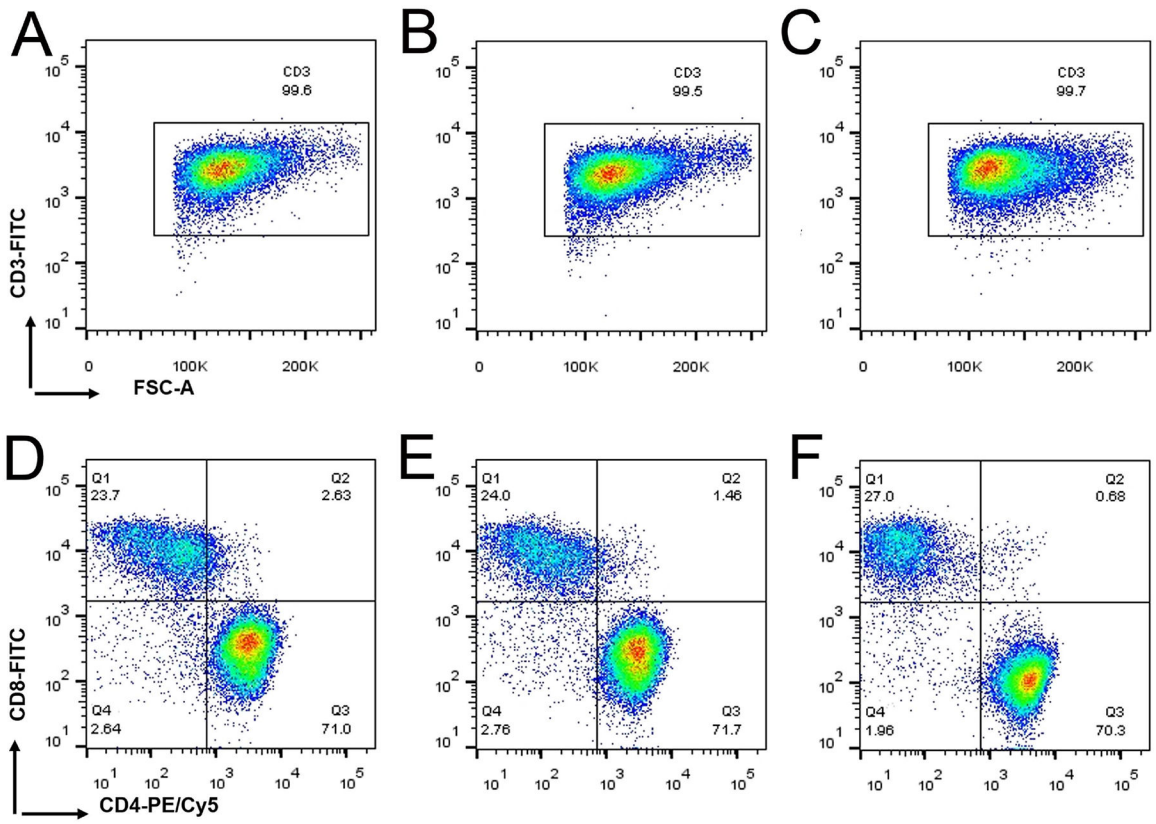

Figure 5.

Phenotype of CAR T cells labeled with TAT-F68-PFC nanoemulsions. Scatter plots confirm pure population of CAR T cells (CD3) (**A-C**). CD3 expression is unaltered after labeling with TATP-F68-PFC (**A**) or TATA-F68-PFC (**B**) nanoemulsions compared to unlabeled cells (**C**). Flow analysis for expression of CD4/CD8 shows a ~ 90/10 ratio of CD4+ to CD8+ positive cells (**D-F**). CAR T cells labeled with TATP-F68-PFC (**D**) or TATA-F68-PFC (**E**) ex vivo exhibit comparable phenotype to unlabeled cells (**F**). FSC-A indicates forward scatter, FITC stands for fluorescein isothiocyanate, and PE/Cy5 is phycoerythrin-cyanine 5.

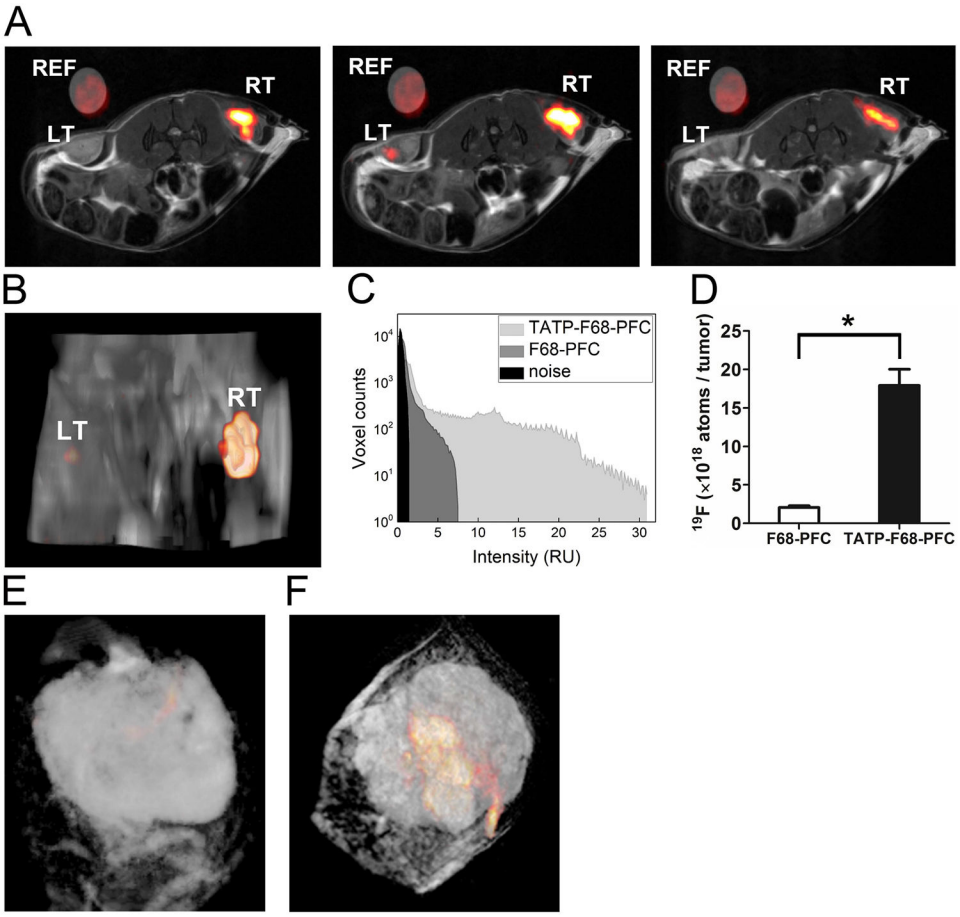

Figure 6.

In vivo ^{19}F MRI signal enhancement in TATP-F68-PFC labeled human CAR T cells. Panel (**A**) displays composite ^{19}F (hot-iron) and ^{1}H (grayscale) contiguous slices of a mouse with bilateral gliomas in the flanks, where the left and right tumor (LT, RT) each received 1×10^{7} CAR T cells labeled with either F68-PFC (control) or TATP-F68-PFC nanoemulsions, respectively. An external capillary reference (REF) is also shown in the field of view consisting of 1:20 dilution of F68-PFC in agarose. Panel (**B**) displays a three-dimensional rendering of the MRI data shown in (**A**). MRI data were acquired at 11.7 T using RARE sequences for ^{19}F and ^{1}H. A histogram of the ^{19}F signal-to-noise ratio for each image voxel in the tumors is displayed in (**C**) and shows sensitivity improvement of the TATP-containing nanoemulsion compared to control. Comparison of apparent ^{19}F atoms per tumor, as measured in vivo for N = 4 mice, is displayed in (**D**) showing ~8-fold sensitivity enhancement (* indicates $p<0.001$) for TAT-F68-PFC nanoemulsions compared to control. To verify intratumoral delivery of CAR T cells, two days after CAR T cell injection, tumors were excised and fixed for extremely high-resolution MRI. Panels (**E, F**) show composite ^{19}F/^{1}H three-dimensional renderings of intratumoral CAR T cells labeled with control and TAT-F68-PFC nanoemulsions, respectively. Data in (**E**, **F**) were acquired at 9.4 T at 100 μm isotropic resolution using RARE (^{19}F) and spin-echo (^{1}H) imaging sequences.